52nd AIAA/ASME/ASCE/AHS/ASC Structures, Structural Dynamics and Materials Conference
 19th
4 - 7 April 2011, Denver, Colorado

AIAA 2011-2172

Damage Resistance and Damage Tolerance of Hybrid Carbon-Glass Laminates

Andrew T. Rhead[1], Hua Shi[2] and Richard Butler[3]
University of Bath, Bath, BA2 7AY, United Kingdom

This paper explores the influence of impact energy and stacking sequence on the damage resistance and damage tolerance of hybrid Carbon Fiber Reinforced Plastic (CFRP) and Glass Fibre Reinforced Plastic (GFRP) hybrid laminates in order to establish their suitability as an alternative to CFRP laminates for use in aircraft structures. Compression after impact tests demonstrate that CFRP/GFRP hybrid laminates display increases in failure stress of up to 32% in comparison to laminates constructed entirely from CFRP. Laminates displaying the highest stresses at failure are those that exploit stacking sequence and GFRP content to prevent delamination from occurring close to the outer surface of the laminate during impact. This eliminates local sublaminate buckling and hence rules out failures due to delamination propagation. A switch to an anti-symmetric buckling mode is noted at low levels of stress in the CFRP baseline laminates subject to higher energy impacts. This mode switch did not occur in the hybrid designs. A previously developed analytical model for assessing damage tolerance of laminates that fail following local buckling induced delamination propagation is shown to be applicable to hybrid laminates.

Nomenclature

A_{11} = Axial stiffness
D_{11} = Longitudinal bending stiffness
D_{22} = Transverse bending stiffness
E_{11} = Longitudinal elastic modulus
E_{22} = Transverse elastic modulus
E_{xx} = Theoretical axial modulus in longitudinal direction
G_{12} = Shear modulus
G_{1C} = Strain energy release rate (SERR)
t = Ply thickness
ε^C = Buckling strain
ε_{th} = Threshold strain below which propagation will not occur
σ^C = Critical buckling stress
σ_{th} = Threshold stress calculated from threshold strain
υ_{12} = Major Poisson's ratio

I. Introduction

The next generation of commercial aircraft will make use of the favorable strength and stiffness properties of Carbon Fiber Reinforced Plastics (CFRP) to provide structural weight savings. However, a number of factors

[1]Research Assistant, Department of Mechanical Engineering, A.T.Rhead@bath.ac.uk
[2]PhD student, Department of Mechanical Engineering
[3]Reader, Department of Mechanical Engineering, R.Butler@bath.ac.uk, AIAA Member

are preventing CFRP from being utilized to its full potential, amongst which Barely Visible Impact Damage (BVID) is of particular significance. BVID leaves surface indentations which are too small to be seen on routine aircraft inspections yet can cause considerable internal damage of which delaminations are the most dangerous component. This is because under compressive loading, delaminations, following the local buckling of the adjacent sub-laminate, can propagate and cause considerable overall strength reductions.

Previous examples of hybridization of laminates aimed at enhancing resistance to BVID formation and/or the damage tolerance properties of laminates include adding aramid interlayers to CFRP laminates to enhance the delamination resistance of the laminate[1, 2] and using GLAss-REinforced Fiber Metal Laminates (GLARE)[3] which have recently entered service in the Airbus A380. Other examples of hybrid laminate construction can be seen in the use of shape-memory alloy/CFRP hybrid laminates to produce property changes using thermal or stress-induced Martenistic transformations[4].

The aim of the work presented in this paper is to determine the effect that adding Glass Fiber Reinforced Plastics (GFRP) layers to CFRP laminates has on the damage resistance and damage tolerance properties of the laminates. GFRP layers are cheaper and less dense than CFRP layers and have previously been added to carbon fiber helicopter blades[5] where their progressive, non-catastrophic failure mechanism (established in load deflection tests) was seen as an advantage for compressive failures where damage was not a factor. Here it is considered that this mechanism may lead to increased strength in the compression after impact (CAI) regime. Hence, the influence of stacking sequence and both position and number of glass layers on hybrid laminate damage resistance and damage tolerance is investigated.

A range of laminates, which have been subject to out-of-plane impacts with various energies, have been assessed experimentally using CAI tests and where applicable theoretically using an analytical Strip model[6]. CFRP laminates with a stacking sequence that has already been identified as being damage tolerant[7] are used as comparative baselines. Experiments were monitored using a Digital Image Correlation (DIC) system which can accurately visualize laminate failure modes and strains.

II. Results

A. Coupon Manufacture

Hybrid CFRP/GFRP coupons were manufactured from carbon (HTA/913C) and glass (GE5/913) pre-preg layers with material properties given in Table 1 and stacking sequences given in Table 2. Three CFRP coupons were also made, two were manufactured from HTA/913C and the third manufactured from AS4/8552 material and previously presented[7].

Table 1. Material properties (*t* is cured layer thickness).

Material	E_{11} (GPa)	E_{22} (GPa)	G_{12} (GPa)	v_{12}	t (mm)	G_{IC} (J/m^2)
GE5/913 (glass)	43.9	15.4	4.29	0.28	0.142	225
HTA/913C (carbon)	135.0	18.5	4.97	0.29	0.134	225
AS4/8552 (carbon)	128.0	10.3	6.0	0.30	0.125	261

Of the various hybrid (H) laminates, H1 had a conventional, homogeneous lay-up which is widely used throughout the aerospace industry as it is suited to ensuring surface and ply continuity across thickness variations during manufacture due to the ease with which ply-drops can be made. All other laminates used variations of a damage tolerant stacking sequence[7] where the variation is a function of the through-thickness placement of GFRP layers. The key principle followed in the damage tolerant laminate design was the placement of less stiff ±45° plies towards the outer surfaces of the laminates to protect a central core of load carrying 0° plies from local buckling and hence delamination propagation. Figure 1 shows plots of theoretical buckling stress σ_C and threshold stress σ_{th} (the stress below which delamination propagation as a result of local buckling will not occur) on a layer by layer basis constructed using the Strip model[8] detailed in Appendix I. A (conservative) 30mm circular delamination was assumed at each interface and it can be seen that the damage tolerant stacking sequences (Figs. 1 (a), (c) and (d)) have higher threshold stress than the homogeneous sequence (Fig. 1 (b)). This effect is particularly magnified for the H3 sequence which has GFRP ±45° outer layers. In addition, hybrid H3 coupons were designed to increase the probability of damage detection by improving impact damage visibility for a given impact energy. This was achieved via placement of glass layers on the outer surface of the laminate. The intention being that better damage

visibility would lead to a lower energy impact threat being designated as sufficient for BVID thus implying the laminate would suffer smaller delaminations leading to an improved CAI strength.

Table 2. Impact energy, stacking sequence, theoretical axial modulus E_{xx}, initial propagation stress σ_{th} and failure stress of coupons. Note that analytical initial propagation stresses σ_{th} are found using the Strip model and are based on delamination sizes from C-scan data.

Laminate ID - Impact energy	Lay-up (C1=AS4/8552, C=HTA/913C, g=GE5/913)	E_{xx} (GPa)	σ_{th} (MPa) Experimental/ Analytical	Experimental Failure Stress (MPa)
CC1-8J	$[(\pm 45_{C1})_4/(90_{C1}/0_{C1})_4]_S$	51	289 / 300	349
CC2-18J	$[(\pm 45_C)_4/(0_C/90_C)_4]_S$	55	-	253
CC3-18J	$[(\pm 45_C)_4/(0_C/90_C)_4]_S$	55	-	250
H1-12J	$[45_C/-45_C/0_C/0_g]_{4S}$	55	284 / 290	284
H1-15J	$[45_C/-45_C/0_C/0_g]_{4S}$	55	247 / 275	276
H1-18J	$[45_C/-45_C/0_C/0_g]_{4S}$	55	233 / 275	288
H2-12J	$[\pm 45_C/45_C/(\mp 45_g)/-45_C/\pm 45_C/(0_C/0_g)_4]_S$	55	-	342
H3-12J	$[(\pm 45_g)_2/(\pm 45_C)_2/((0_C)_3/0_g)_2]_S$	65	-	343
H3-18J	$[(\pm 45_g)_2/(\pm 45_C)_2/((0_C)_3/0_g)_2]_S$	65	-	335
H4-8J	$[(\pm 45_C)_4/(0_C/0_g)_4]_S$	55	-	404
H5-8J	$[(\pm 45_C)_4/(0_g/0_C)_4]_S$	55	-	403
H5-12J	$[(\pm 45_C)_4/(0_g/0_C)_4]_S$	55	-	>382*

*Test was halted before final failure occurred to assess propagation of damage from the impact site.
- Indicates the failure mode of the laminate meant the Strip model was not applicable.

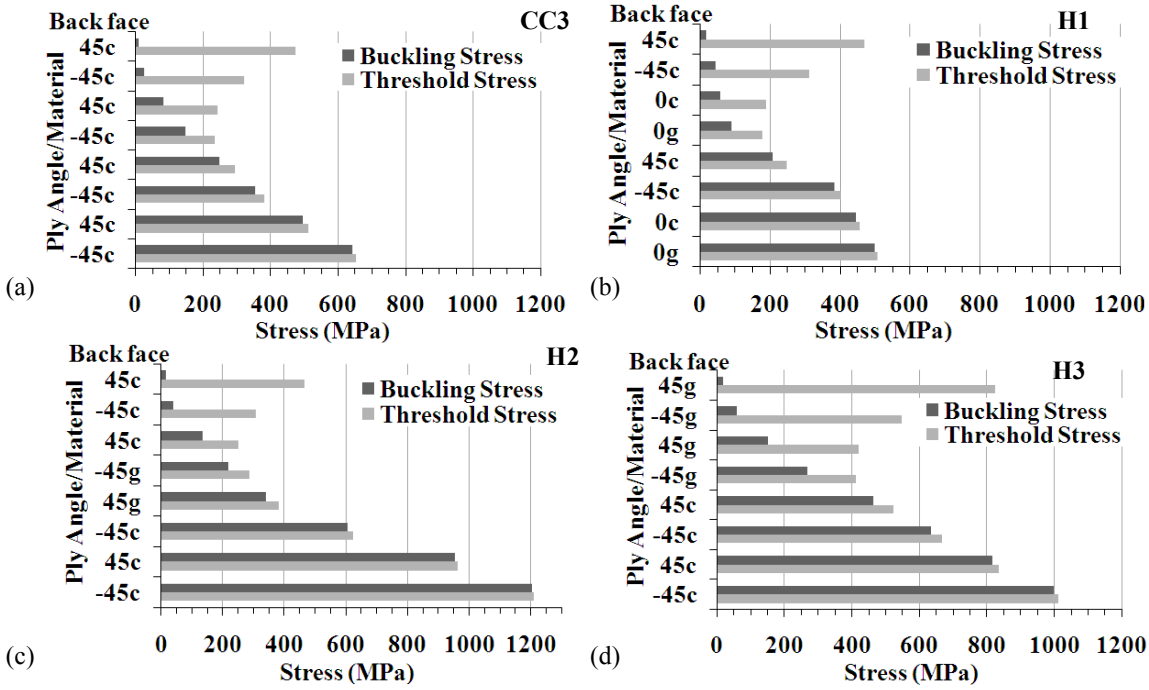

Figure 1. Plots of theoretical buckling stress and threshold stress for individual layers assuming a 30mm circular delamination at each interface for stacking sequences (a) CC3, (b) H1, (c) H2 and (d) H3.

B. Impact Results

Coupons were subjected to single 8, 12, 15 or 18J out-of-plane impacts at their (plan form) center using an instrumented impact test machine employing a 16mm diameter tup. During impact, coupons were clamped over a 75mm x 125mm test window (the long edge being aligned parallel to the 0^o fiber axis) as prescribed by the ASTM standard[9]. The extent of BVID was measured using an ultrasonic C-scan system, see Fig. 2.

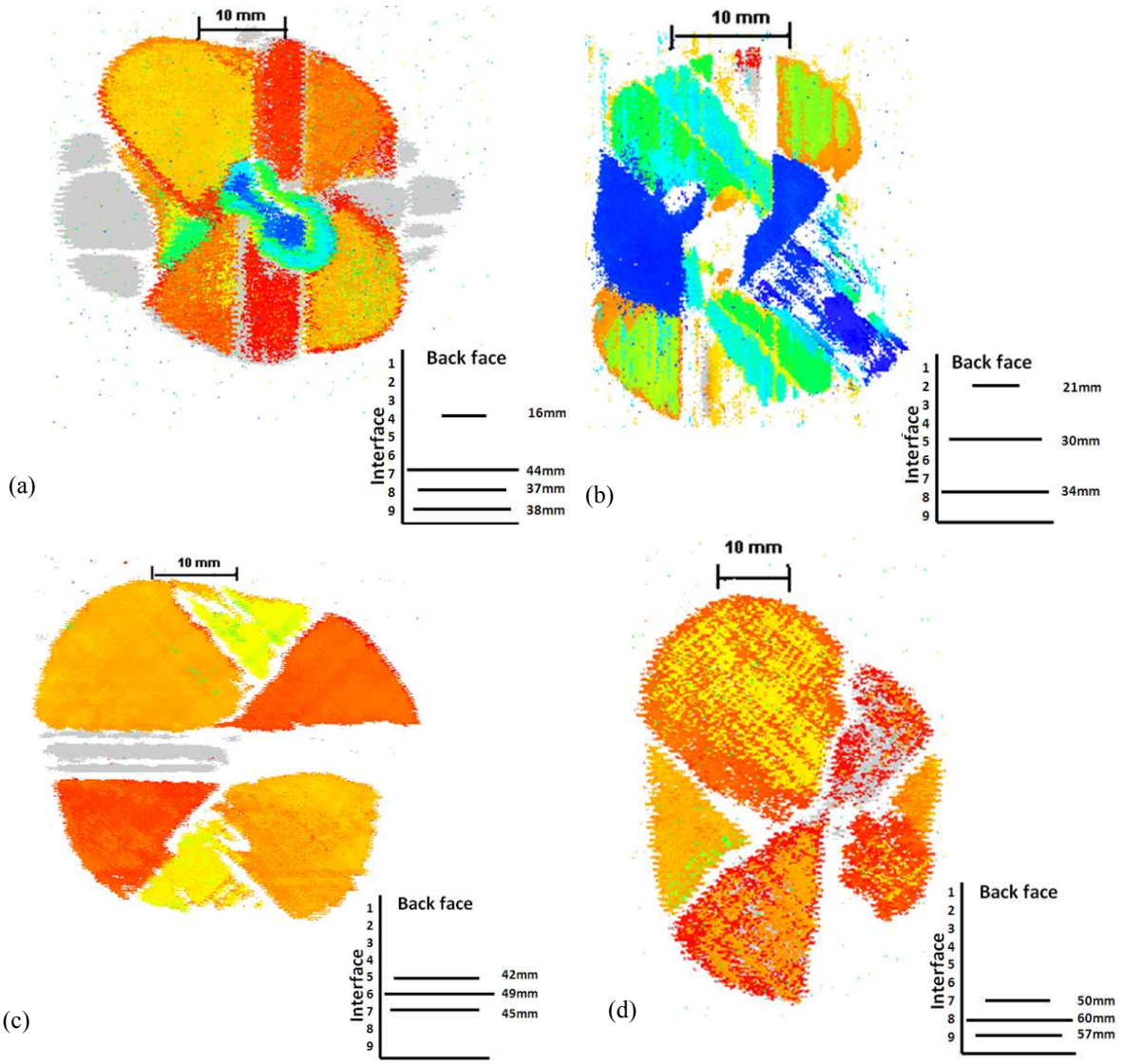

Figure 2. C-scan images of delaminations caused by impact in (a) CC3-18J, (b) H1-18J, (c) H2-12J and (d) H3-18J laminates. Delamination coloring indicates distance of delamination from the back face and is consistent across images. Insets show the maximum diameter of a circle that contains the full delaminated area for each delaminated interface. In each the 0^o fiber axis is vertical.

The high attenuation to ultrasound waves exhibited by the GFRP layers meant that clarity of delamination edges in the hybrid laminates was not as good as that seen in the CFRP laminates (contrast Figs. 2.(a) and (b)). Hence the determination of delamination size was not as accurate for the hybrid laminates. Note however, that the determination of through-thickness position of delaminations using time-of-flight data from the C-scan is unaffected by this attenuation. Table 3 gives the diameter of circles containing delamination at individual interfaces in the experimental laminates for the first nine interfaces from the back face. This provides a delamination diameter for all interfaces at which local-buckling and hence delamination propagation could possibly occur (contrast σ_C predictions

in Fig. 1 with experimental failure stresses in Table 2). Diameters are determined from analysis of individual delaminations revealed by C-scans of the impacted laminates, see Fig. 1. Note that the largest delamination for coupon CC2-18J had a diameter of 41mm and occurred at the 12th interface. Impact energies associated with the delamination distributions are noted in the laminate ID in Table 3.

Table 3. Diameters of circles (in mm) containing delamination damage at individual interfaces as defined by C-scans of each coupon. Maximum diameters are underlined. Circles indicate interfaces at which local propagation was predicted by the Strip model.

Laminate ID.	Back Face	Interface number 1	2	3	4	5	6	7	8	9
CC1-8J			13	(13)	15	11	10	20	16	37 -
CC2-18J		-	16	-	-	-	-	20	-	-
CC3-18J		-	11	-	16	-	-	44	37	38
H1-12J		-	(26)	-	-	20	31	29	-	-
H1-15J		-	33	-	-	(30)	30	-	30	-
H1-18J		-	21	-	-	(30)	-	-	34	-
H2-12J		-	-	-	-	42	49	45	-	-
H3-12J		-	-	-	-	-	-	13	57	54
H3-18J		-	-	-	-	-	-	50	60	57
H4-8J		-	-	-	-	-	-	32	35	37
H5-8J		-	-	-	-	-	-	33	37	36
H5-12J		-	-	-	-	-	54	-	59	50

"-" implies little or no delamination damage

C. Compression After Impact Results

Prior to compression testing, laminates were placed in a compression fixture with an integrated circular anti-buckling guide of internal diameter 85mm, see Fig. 3. Tests consisted of applying axial compression under displacement control at 0.1 mm/min until local delamination propagation and/or global failure occurred. The back (non-impact) faces of the coupons were covered in a random speckle pattern to allow buckling modes and failure sequences to be visualized (following post-processing) using the DIC system. This system employs a pair of stereo cameras to produce plots of out-of-plane displacement relative to a reference image taken under zero load. To ensure specimens were correctly aligned, strains were recorded throughout the tests by two pairs of vertically aligned back-to-back strain gauges. See Fig. 3 for a schematic diagram of strain gauge placement.

Failure stresses and propagation stresses are given in Table 2 and were calculated by dividing the corresponding loads by the cross-sectional area of each coupon. Table 2 also gives analytical predictions of propagation stresses. Failure of the laminates occurred via one of the three following mechanisms, determined from a combination of DIC images (Fig. 4) and load vs. strain plots (Fig. 5). For the CC1 and H1 coupons failure was brought about by propagation of a delamination following local buckling as shown by the very localized coloring and tight contours in Figs. 4(c) and (d). Propagation is also indicated by small discontinuities (in comparison to the discontinuities seen in Fig. 5(a)) which are highlighted by a circle on the corresponding load vs. strain plot, see Fig. 5(b). The circle of Fig. 4(c) indicates the boundary of the area containing the initially buckled region, propagation occurs once the buckled region spreads outside this circle.

For the CC2 and CC3 coupons, failure followed a change in global buckling mode shape from that seen in Fig. 4(a) to a fully anti-symmetric mode contained within the confines of the anti-buckling guide seen in Fig. 4(b).The large discontinuities seen on the load vs. strain plot in Fig. 5(a) are co-incident with the sudden jump to a fully anti-symmetric buckling mode from an intermediate asymmetric mode that developed at loads between those shown in Figs. 4(a) and (b). The third failure mechanism noted in the remaining laminates, see Figs. 4(e) and (f), was that of material failure induced by (symmetrical) global buckling. Note the non-localized, more slowly changing pattern of colors in Figs. 4(e) and (f) seen for global buckling in comparison to the central region of Figs. 4(c) and (d). Load vs. strain plots for symmetric globally buckled coupons show a steady divergence of strain gauge curves (see Fig. 5(c)) consistent with global buckling.

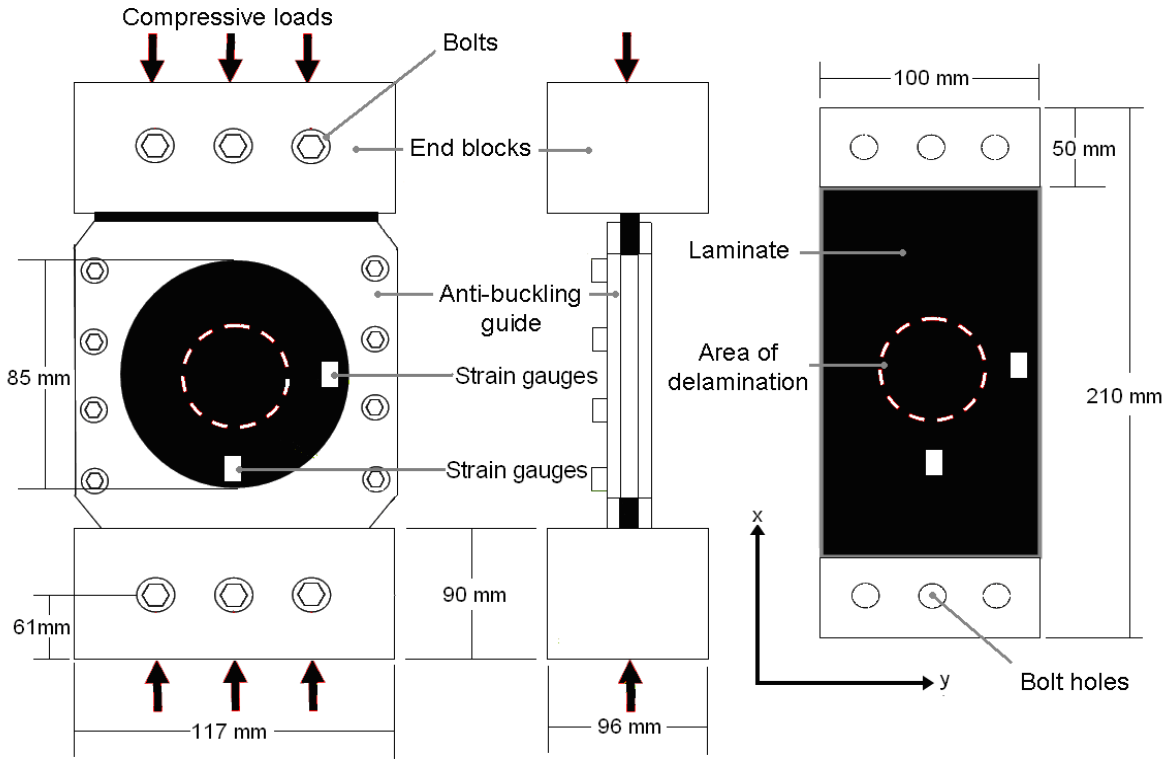

Figure 3. Experimental set-up and coupon details.

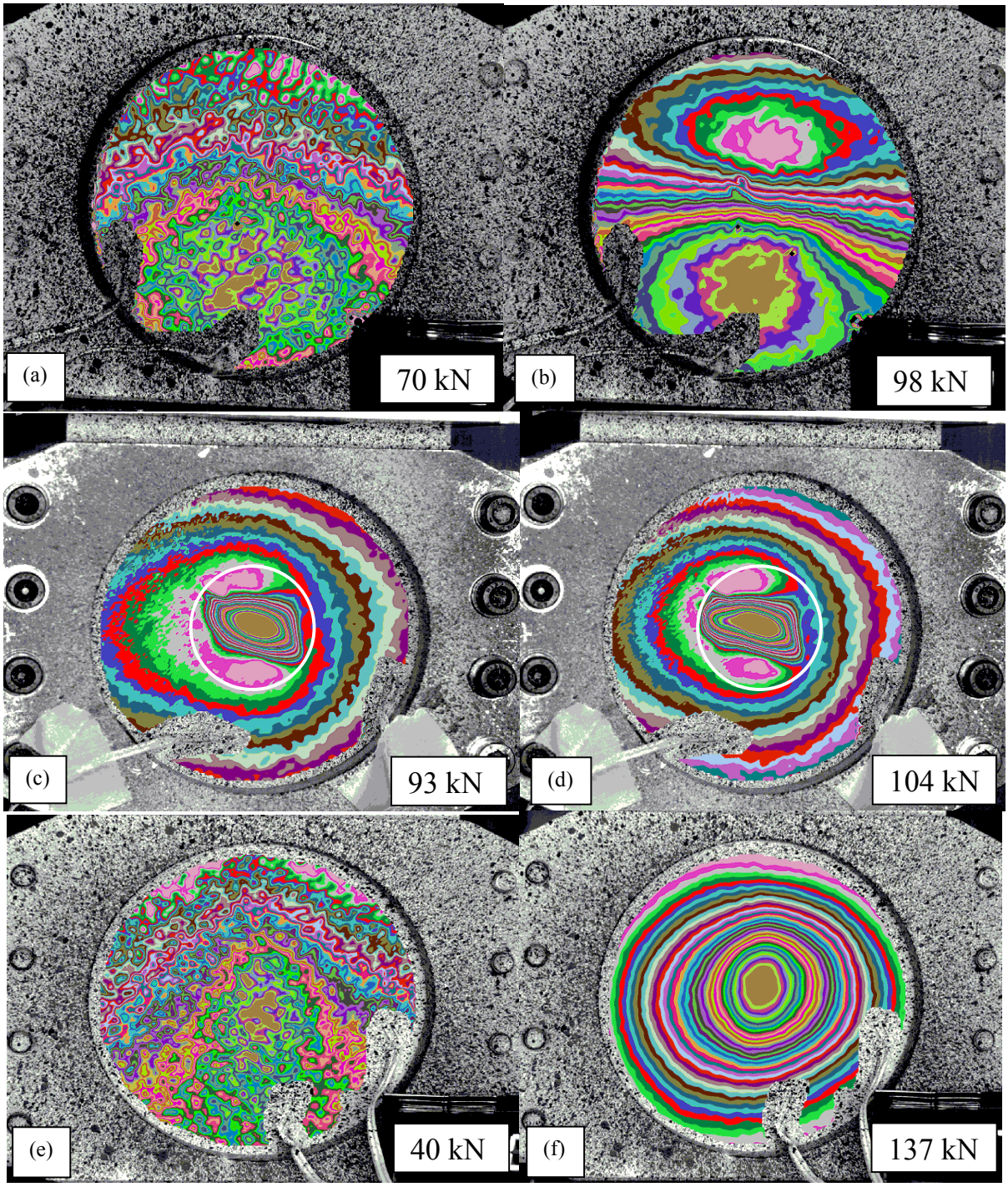

Figure 4. DIC images during CAI testing with colors indicating out-of-plane displacement from an initial unloaded state. (a) Global buckling prior to (b) anti-symmetric global buckling in CC2-18J. (c) Local buckling above a delamination and (d) following propagation in H1-18J. (e) and (f) Evolution of the global buckling of H3-18J.

(a)

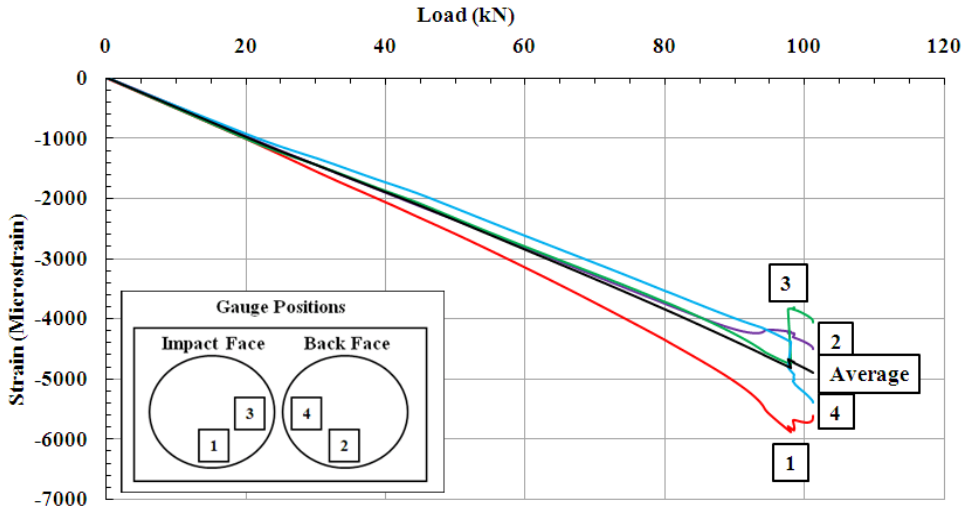

(b)

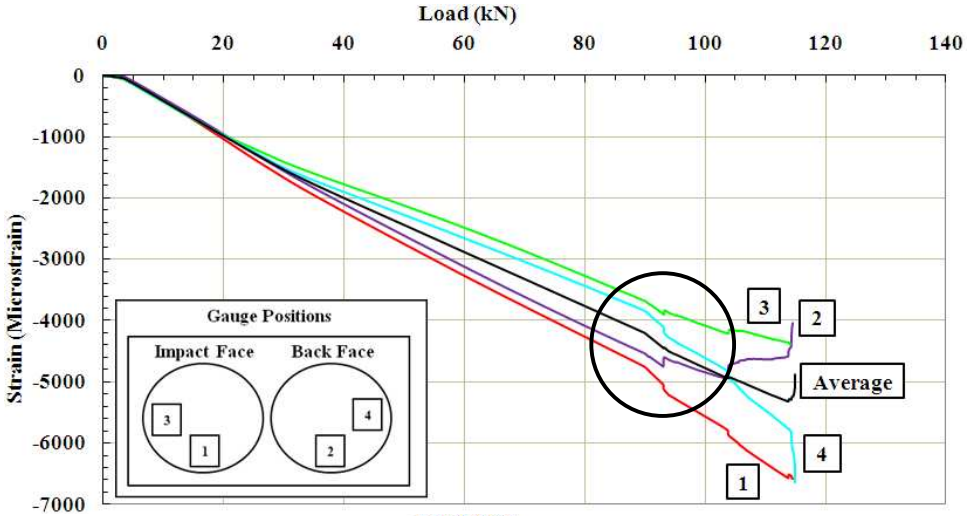

(c)

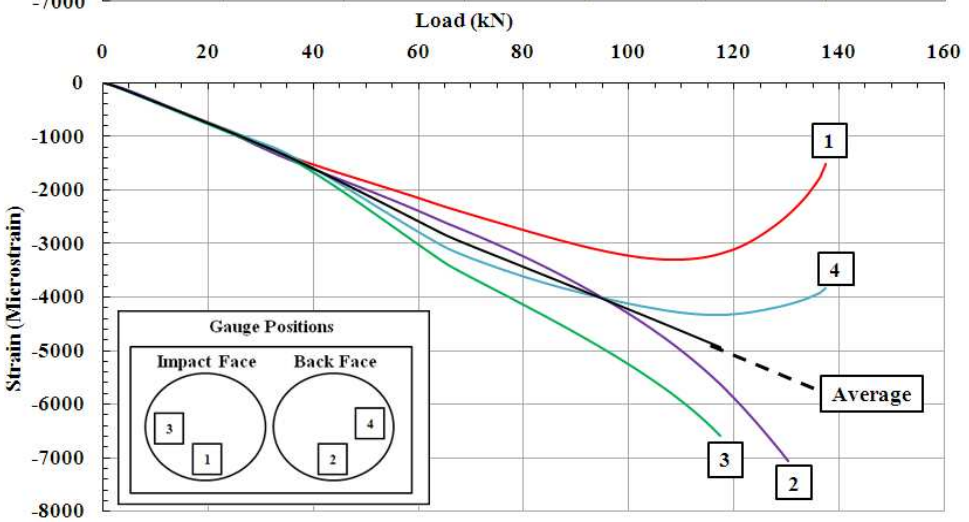

Figure 5. Load vs. Strain plots for compression (CAI) testing of laminates: (a) CC2-18J, (b) H1-18J and (c): H3-18J. The circle in (b) highlights discontinuities associated with delamination propagation.

III. Discussion

A. Damage Resistance

A comparison of C-scan results in Table 3 for coupons with 12J impacts (H2, H3 and H5) and identical stacking sequences (ignoring layer material) suggests that if glass layers are included, their through-thickness positioning has a significant effect on delamination morphology, independent of the overall percentage of glass layers. The through-thickness position of the largest delamination is also affected. A detailed discussion of damage morphology follows.

1. Delamination size

Stacking sequence and in particular blocking of plies into either (45_C/-45_C) and (0_C/0_g) or (45_C/-45_C) and (-45_g/45_g) groups has a significant effect on the maximum delamination diameter. A comparison of damage distributions for all coupons clearly demonstrates this effect as the largest delaminations occur in the region where these blocks meet, i.e. interface 8 for all coupons except H2 where blocking of (45_C/-45_C) and (-45_g/45_g) plies occurs at the 5th interface and H1 where all even interfaces separate blocks of (45_C/-45_C) and (0_C/0_g) plies. Blocking produces interfaces where sharp contrasts in dominant ply direction and thus significant differences in the direction of principal bending stiffness occur. These incompatibilities result in large interlaminar stresses.

Hybrid laminates H2, H3, H4 and H5 displayed larger maximum delaminations than both H1 and the fully CFRP laminates. This is partially due to the increased energy of the impacts delivered to some coupons and the affect of ply-blocking noted above but is also an effect of the placement of glass layers, see below. Multiple blocks of plies in H1 result in multiple areas of large interply shear stress across which the total energy from impact can be dispersed resulting in more delaminations with individually smaller areas.

2. Delamination distribution

The comparatively large number of delaminations in H1 (see Fig. 2(b) and Table 3) is due to the dispersed stacking sequence (as seen previously[7]) creating multiple through thickness areas (block of plies) with considerably different bending stiffnesses as noted above. In contrast to H1, which has interspersed carbon and glass layers, where the first delamination occurs at the 2nd interface from the back face (no matter what impact energy), the first delamination from the back face for the other hybrid laminates does not occur before the 5th interface, see Table 3. This is because when considered with regard to the shape of the ASTM impact window and the resulting relative lengths of the 45° fibers, pairs of ±45° plies are relatively compliant compared to quasi-isotropic (i.e. $[45/0/-45/90]_2$) outer ply stacking sequences during impact and thus relieve interlaminar stresses. The use of glass layers in combination with a damage tolerant stacking sequence[7], which places compliant pairs of ±45° plies to the outside of the laminate, has amplified an effect of the stacking sequence which causes a high proportion of the total area of delamination to occur closer to the mid-plane of the laminate[7]. This means little or no delamination occurs in the critical through-thickness region (approximately 20% of laminate thickness from the back face[10], see Table 3) where local buckling and delamination propagation can occur.

The central delamination distributions seen in H3, H4, H5 and to some extent H2 are a product of the damage resistant aspects of the stacking sequences used and the ductility and low modulus of the GFRP layers. It is evident that centrally located glass layers draw damage to the centre of laminates H2-H5, see Table 3. This is likely to be due to the reduced shear rigidity of the GFRP layers, leading to delamination caused by high shear stress in the resin rich ply interfaces.

Impacts to H3 and H4 coupons resulted in the least near-surface delaminations, though in the latter case this was most likely a consequence of the low impact energy particularly when the damage distribution of H5-12J (which has a very similar stacking sequence) is taken into account.

3. Damage visibility

As anticipated, impact damage visibility and hence BVID detectability was improved by the GFRP layers on the outside of the H3 laminate. This was due to the formation of opaque through-thickness regions in the outer glass plies (particularly on the back face) following impact that were easily distinguished from the intact glass regions that remained translucent. However, external aircraft surfaces are painted and thus this increased visibility will only apply to internal surfaces. Note also that in general, hybrid laminates have a more elastic response to impact than CFRP laminates due to the lower bending stiffness of the former, see Table 4. This is likely to result in smaller visible dents in the hybrid laminates following impact which may hamper impact detection. This would result in a higher energy impact being required to create BVID in hybrid laminates than that required for CFRP laminates. The authors conclude though that although damage visibility may decrease for hybrid laminates the significant increases

seen in damage tolerance (see Table 3) would be worth the sacrifice particularly if a non-visual damage detection system/method were implemented.

Table 4. Buckling modes and overall bending stiffness of Table 2 laminates in longitudinal (D_{11}) and (D_{22}) transverse direction.

Coupon	D_{11} (kNmm)	D_{22} (kNmm)	Buckling mode
CC2/CC3	340	322	Overall (Anti-symmetric)
H1	455	237	Local (Sublaminate)
H2	335	262	Overall (Symmetric)
H3	291	199	Overall (Symmetric)
H4	366	293	Overall (Symmetric)
H5	350	293	Overall (Symmetric)

B. Damage Tolerance

Despite the use of an anti-buckling guide during compression tests, global buckling was detected via strain gauge plots and DIC images for all coupons and was the final failure mechanism for all coupons except, CC1-8J, H1-8J, H1-12J and H1-18J. For these coupons DIC images indicated the presence of near surface delaminations that allowed formation of local buckles under compressive loading which subsequently caused delamination propagation thus weakening the laminate and causing failure. The local buckling and delamination propagation seen in the above laminates meant it was possible to apply the analytical Strip model. Analytically predicted stresses were within 4%, 2%, 10% and 15% of the experimental values for CC1-8J, H1-8J, H1-12J and H1-18J, respectively, demonstrating the applicability of the modeling methodology to hybrid laminates.

In contrast to the CC1 and H1 laminates, a comparison of DIC images and load vs. strain plots for the fully CFRP laminates indicates an anti-symmetric global buckling mode caused the failure of CC2 and CC3 at reduced levels of applied stress. It is believed this anti-symmetric mode was promoted by through-thickness shear deformation at the center of the damaged laminate. This mode is thought to have been enabled by intraply cracking in the 90^o plies allowing the laminate to deform much more easily than would be allowed by the intact central 0^o plies in the hybrid laminates. It is thought this mechanism did not occur in the CC1 coupon due to the lower impact energy sustained by this laminate producing less damage.

As a consequence of the combination of GFRP layers and damage tolerant stacking sequences in the hybrid laminates H2, H3, H4 and H5 delamination was contained to a through-thickness region near the mid-plane of the laminate, see Table 3. By constraining delamination formation during impact to the center of the laminate hybrid laminates H2, H3, H4 and H5 (i) prevented local buckling and thus delamination propagation and (ii) delayed global buckling by keeping the outer layers adhered thus maintaining the bending stiffness of the laminate. Table 2 clearly indicates that hybrid laminates H2, H3, H4 and H5 have the potential to offer improvements of up to 32% in damage tolerant strength compared with the CFRP laminates of similar stacking sequence and similar impact energies. Indeed coupon H5-12J failed at a higher stress than the strongest CFRP laminate CC1-8J despite being subject to a 50% higher energy impact. Note also that the H3-18J coupon failed at only 4% lower stress than the CC1-8J coupon despite an impact energy 2.2 times that received by the CC1-8J coupon. A comparison of results in Tables 2 and 3 shows that local buckling propagation can be prevented via stacking sequence selection in combination with the addition of GFRP plies and that this combination led to hybrid laminates outperforming carbon laminates.

An inspection of results in Table 2 reveals that increased impact energy had little effect on the maximum stress to failure of the hybrid laminates in contrast to the CFRP laminates where an increase in impact energy produced a considerably lower failure stress due to a change in failure mechanism.

IV. Conclusion

The experiments conducted in this paper provide benchmark test results for comparison of damage tolerance and damage resistance properties of CFRP and CFRP/GFRP hybrid laminates that can be used to validate other analytical models in future.

Hybrid laminates are shown to display failure stresses up to 32% greater than CFRP laminates with identical impact energies. However, this must be considered in the context of BVID which is described by dent depth and

diameter. It may be the case that BVID is reached for carbon coupons at a lower impact energy than for hybrid coupons and thus an impact energy comparison may be invalid. This argument is somewhat degraded by the fact that the some coupons failed at a higher stress than the strongest CFRP laminate despite being subject to 50% higher energy impact.

The extent to which the hybrid laminates outperformed the CFRP laminates was dependent on the stacking sequence and through-thickness positioning of glass layers. Laminates displaying the highest stresses at failure were those that exploited the above to prevent delamination from occurring close to the outer surface during impact. This in turn prevented local sublaminate buckling under compression and hence prevented failures due to delamination propagation. A change from a symmetric to an anti-symmetric global buckling failure noted in some of the CFRP laminates subject to higher energy impacts, was not displayed by the hybrid designs.

A previously developed analytical model for predicting the strain below which propagation of locally buckled delaminations will not occur is shown to be applicable to hybrid laminates.

Appendix I.

Analytical Strip Model

The authors have previously presented a simple, Strip model[8] to predict critical threshold values of applied strain below which initial local buckle-driven propagation of a delamination will not occur. Delamination areas below the sublaminate under investigation are modeled as circles to produce a simple approximation of the damage in a laminate, as viewed on a C-scan. The Strip model is then used to calculate the compressive threshold strain ε_{th} for the associated sublaminate, ε_{th} is given by,

$$\varepsilon_{th} = \varepsilon^{C}\left(-1+\sqrt{4+\frac{2G_{IC}}{A_{11}(\varepsilon^{C})^{2}}}\right) \tag{1}$$

where ε^{C} is the buckling strain of the circular sublaminate adjacent to the delamination, calculated using the 2D infinite strip program [11], G_{IC} is the strain energy release rate required to cause Mode I fracture in the matrix material and A_{11} is the axial stiffness of the sublaminate. The propagation strain is converted to a propagation stress σ_{th} using the theoretical axial modulus E_{xx} of the laminate. The model, which makes a number of simplifying assumptions, has been successfully applied to determine stacking sequences that are damage tolerant, and to highlight whether propagation is stable or unstable[6]. It has also been recently applied for comparison with experimental testing and finite element analysis of a number of laminates containing artificial delaminations[8].

Acknowledgments

The authors are grateful to Agusta-Westland for supply of material. The first author is currently supported by the EPSRC (Grant No.EP/H025898/1), Airbus Operations and GKN Aerospace.

References

[1]Yadav, S. N., Kumar, V., Verma, S. K., "Fracture Toughness Behaviour of Carbon Fiber Epoxy Composite with Kevlar Reinforced Interleave," *Materials science & engineering*, Vol.132, 2006, pp.108-12.

[2]Wardle, M., W., "Impact Damage Tolerance of Composites Reinforced with Kevlar Aramid Fibers," *Jpn Soc Compos Mater*, 1982, pp. 837-44.

[3]Botelho, E. C., Silva, R., A., Pardini, L. C., Rezende, M. C. "A Review on the Development and Properties of Continuous Fiber/Epoxy/Aluminum Hybrid Composites for Aircraft Structure," *Material Research*, Vol. 9, 2006, pp. 247-56.

[4]Wei, Z. G., Sandstrőm, R., "Review Shape memory materials and Hybrid Composites for Smart Systems – Part II Shape-Memory Hybrid Composites," *Journal of Materials Science*, Vol. 33, 1998, pp. 3763 – 83.

[5]Middleton, D. H. (ed.), *Composite Materials in Aircraft Structures*, Longman Scientific & Technical, Singapore, 1990, pp. 307.

[6]Rhead, A. T., Butler, R., Hunt, G. W., "Post-buckled Propagation Model for Compressive Fatigue of Impact Damaged Laminates," *Int J Solids Struct*, Vol. 45, No. 11, 2008, pp. 4349–61.

[7]Rhead, A. T., Butler, R., Baker, N., "Analysis and Compression Testing of Laminates Optimised for Damage Tolerance," *Appl Compos Mater,* DOI: 10.1007/s10443-010-9153-z.

[8]Butler, R., Rhead, A. T., Liu, W., Kontis, N., "Compressive strength of delaminated aerospace composites" *Phil. Trans. R. Soc. Lond. A*. (under review).

[9]"Standard test method for measuring the damage resistance of a fiber-reinforced polymer matrix composite to a drop-weight impact event," ASTM Designation: D7136 / D7136M - 07 doi:10.1520/ D7136_D7136M-07. 2009.

[10]Melin, G. L., Schön, J., "Buckling behaviour and delamination growth in impacted composite specimens under fatigue load: an experimental study," *Composites Science and Technology*, Vol.61, 2001, pp.1841-1852.

[11]Wittrick, W. H., Williams, F. W., "Buckling and vibration of anisotropic or isotropic plate assemblies under combined loadings," *Int J Mech Sci,* Vol. 16, 1973, pp. 209–39.